

## Article

# Rapid, Minimally Invasive Prediction of Starch and Moisture Content in Saffron Corms Using Visible–Near-Infrared Spectroscopy Combined with Machine Learning

Mahdi Faraji <sup>1,2</sup>, Saham Mirzaei <sup>3</sup> , Rasoul Rahnemaie <sup>1,\*</sup> , Shahriar Mahdavi <sup>4</sup>, Alessandro Pistillo <sup>2</sup>, Giuseppina Pennisi <sup>2</sup> , Afsaneh Nematpour <sup>2</sup> , Andrea Strano <sup>2</sup> , Michele Consolini <sup>2</sup>, Francesco Spinelli <sup>2</sup>  and Francesco Orsini <sup>2</sup> 

<sup>1</sup> Department of Soil Science, Tarbiat Modares University, Tehran 14115-336, Iran; mahdifaraji@modares.ac.ir

<sup>2</sup> DISTAL—Department of Agricultural and Food Sciences, Alma Mater Studiorum—Università di Bologna, Viale Fanin 44, 40127 Bologna, Italy; alessandro.pistillo2@unibo.it (A.P.); giuseppina.pennisi@unibo.it (G.P.); afsaneh.nematpour@unibo.it (A.N.); andrea.strano3@unibo.it (A.S.); michele.consolini5@unibo.it (M.C.); francesco.spinelli3@unibo.it (F.S.); f.orsini@unibo.it (F.O.)

<sup>3</sup> Institute of Methodologies for Environmental Analysis, Italian National Research Council, 85050 Potenza, Italy; sahammirzaei@cnr.it

<sup>4</sup> Department of Soil Science, Faculty of Agriculture, Malayer University, Malayer 65719-95863, Iran; sh.mahdavi@malayeru.ac.ir

\* Correspondence: rahnemaie@modares.ac.ir; Tel.: +98-(0)21-4478-75554

## Abstract

The starch and moisture content of saffron corms are critical indicators of their flowering potential and yield. This study investigated the use of rapid, minimally invasive VNIR reflectance spectroscopy measurement to assess these parameters. The measurements were used to develop predictive models through four machine learning algorithms (PLSR, RF, SVR, and GPR). Spectral data were obtained from 130 fresh corm samples. Wavelength analysis identified key starch-sensitive intervals (~930–1000 nm and ~1150–1220 nm) and a broad moisture-sensitive region (~900–1350 nm). Among the evaluated models, the combination of the multiplicative scatter correction pre-processing method and Gaussian process regression (MSC-GPR) demonstrated the optimal predictive performance for water content ( $R^2 = 0.92$ , RMSE = 0.71%, RPD = 4.56, RPIQ = 5.37), and the combination of the MSC method and partial least squares regression (PLSR-MSC) demonstrated moderate performance for starch content ( $R^2 = 0.73$ , RMSE = 28.7 mg g<sup>-1</sup>, RPD = 2.14, RPIQ = 2.81, dry weight). These results demonstrate the viability of VNIR spectroscopy as a minimally invasive tool for the pre-planting assessment of saffron corm quality under laboratory conditions. The method provides a laboratory-based framework for corm screening and selection, with potential for future adaptation to field settings using portable spectrometers following expanded calibrations and advanced modeling techniques.

**Keywords:** reflectance spectrometry; corm screening; chemometrics; pre-planting quality assessment; PLSR



Academic Editor: Yang Liu

Received: 2 March 2026

Revised: 2 April 2026

Accepted: 13 April 2026

Published: 17 April 2026

**Copyright:** © 2026 by the authors.

Licensee MDPI, Basel, Switzerland.

This article is an open access article distributed under the terms and conditions of the [Creative Commons Attribution \(CC BY\) license](https://creativecommons.org/licenses/by/4.0/).

## 1. Introduction

Saffron (*Crocus sativus* L.), the world's most valuable spice, derives its economic and medicinal value from secondary metabolites such as crocin, picrocrocin, and saffranal [1,2]. As a sterile triploid plant, saffron is propagated exclusively through daughter corms [3,4]. The mother corm is not merely a reproductive unit but a critical storage organ, whose

physiological state dictates the plant's capacity for flowering and the vigor of the next generation [5]. Consequently, the internal quality of the planting corm is a primary determinant of field performance and final yield [6].

The saffron corm mobilizes internal reserves to initiate flowering and sustain early growth. Starch, which constitutes the primary storage carbohydrate reserve, is essential for metabolic activities and dormancy breaking [7,8]. Since flowering often occurs before any significant leaf development, the initial phases of floral and vegetative growth are strongly reliant on these stored compounds [9]. Therefore, quantifying starch and moisture content provides a direct proxy for the corm's physiological maturity and flowering potential, offering a valuable metric for rapid screening of corms before planting [10–12].

In Iran, the leading global producer, saffron yield is facing increasing pressure from both climate change and soil degradation [13,14], as well as limited access to large and healthy corms [4]. Accordingly, improving corm quality management is a strategic task for improving yield stability and sustainability of saffron cultivation in all countries [15]. This challenge requires practical methods to assess corm composition. Traditional techniques, such as High-Performance Liquid Chromatography (HPLC) and Gas Chromatography (GC), while accurate, are time-consuming, expensive, and destructive, rendering them impractical for large-scale screening [16,17]. Therefore, there is a pressing need for the development of rapid, accurate, and non-destructive methods to fill the gap between laboratory precision and field-scale application [18].

Visible–near-infrared (VNIR) spectroscopy (350–2500 nm) has been widely used in agriculture for measuring cereal protein content and fruit ripeness grade [19], controlling food industry input materials [20], assessing crop quality [21], monitoring plant health [22,23], and predicting internal plant components [24]. This method can potentially be used for rapid and minimally invasive assessment of corm quality by detecting the molecular vibrations of O–H, C–H, and N–H bonds. Chemometric methods, such as partial least squares regression (PLSR), effectively translate spectral data into reliable quantitative models capable of predicting moisture content and carbohydrate composition [25,26]. While VNIR has been used to assess saffron stigma quality and detect adulteration [27], recent hyperspectral studies have shown that starch and moisture in saffron corms can be predicted under specific conditions [28]. However, the direct and targeted prediction of these two key traits in healthy saffron corms using a simple VNIR approach remains largely unexplored.

This study aims to address this gap by developing and validating machine learning models based on VNIR spectroscopy data for the rapid, accurate, and minimally invasive prediction of starch and moisture content in saffron corms. The full-scale goal is to provide a practical decision-making framework for screening and grading corms before cultivation. Simultaneous assessment of starch and moisture also provides producers with a more comprehensive picture of the corm's physiological status and can strengthen corm planting and maintenance management towards precision agriculture and sustainable production.

## 2. Materials and Methods

### 2.1. Plant Material and Sample Preparation

Saffron corms with a commercial caliber size of 9–10 cm in circumference (mean fresh weight about 12 g) were obtained from the supplier Roco Saffron (Noordwijkerhout, The Netherlands; <https://www.rocosaffron.com/>) on 15 July 2024 (Figure 1). Upon delivery, the corms were stored at  $25 \pm 2$  °C in darkness conditions at the Department of Agricultural and Food Sciences (DISTAL) of Alma Mater Studiorum University of Bologna (UNIBO), Emilia-Romagna, Italy. Two groups of corms were analyzed. In the first group, fresh corms were weighed and assigned a unique ID. The VNIR spectra were then collected from each intact corm. Subsequently, the same corms were oven-dried at 60 °C to constant weight,

ground into a fine powder, and used for reference starch determination. In the second group, corms were weighed, oven-dried under the same conditions, ground into powder ( $\leq 0.5$  mm particle diameter), and VNIR spectra were acquired from the resulting powder. Spectra from dried corms were collected for a small subset of 12 samples. These measurements were used only for visual inspection and comparison of the dried-sample spectral patterns. They were not included in any quantitative analysis or model development, and no spectral pre-processing was applied to these data.



**Figure 1.** (a) Saffron corms (*Crocus sativus* L.) obtained from the supplier Roco Saffron; (b) corm size classification and separation of a commercial caliber of 9–10 cm used for measurement.

## 2.2. Reference Measurements

Moisture content was determined gravimetrically. The percentage moisture content relative to the initial fresh weight was calculated using the mass loss after oven-drying at 60 °C to constant weight. Total starch content was determined using the Megazyme Total Starch Assay Kit (K-TSTA-100A) (Neogen Corporation, Lansing, MI, USA) following the manufacturer's instructions. Accordingly, 100 mg of dried corm powder was assessed for starch content in duplicate. The assay employs enzymatic hydrolysis of starch with thermostable  $\alpha$ -amylase followed by amyloglucosidase (AMG). Eventually, it was quantified by colorimetric determination of the released glucose using the GOPOD (glucose oxidase/peroxidase) reagent. Absorbance was measured at 510 nm. UV-Vis spectrophotometric analyses were performed using a Biochrom Libra S80PC double-beam spectrophotometer (Biochrom Ltd., Cambridge, CB25 9PE, UK), controlled via PC. Starch content was calculated according to the manufacturer's instructions.

## 2.3. Saffron Corm Preparation and VNIR Spectroscopy

For the spectroscopic analysis, fresh saffron corms were used. A total of 130 fresh corm samples allowed for the observation of spectral features influenced by the inherent moisture content. For 12 corms (different from 130 fresh samples), spectroscopy was done for dried powdered samples, enabling the removal of moisture-related spectral variations. Before spectroscopy, each corm was weighed with a scale with 4 decimals of precision. The spectral measurement was done at the Italian National Research Council (CNR-ARTOV), Rome, Italy. VNIR reflectance spectra were acquired using an ASD FieldSpec-4 spectrometer (Analytical Spectral Devices Inc., Boulder, CO, USA), covering the wavelength range of 350–2500 nm. In order to obtain spectra from fresh and healthy corms, the entire tunic was removed. This step was necessary to eliminate the detrimental effect of the corm's skin on the spectroscopy analysis. All spectra were collected on 12 August 2024, under natural light conditions between 11:00 and 13:00 (local time). The sensor was mounted on a tripod at a nadir position, with the lens positioned 7 cm above the sample surface. To reduce the sensor's field of view (FOV), an 8-degree lens was used. White references (Spectralon<sup>®</sup>) were taken before each measurement to account for light variation (Figure 2).

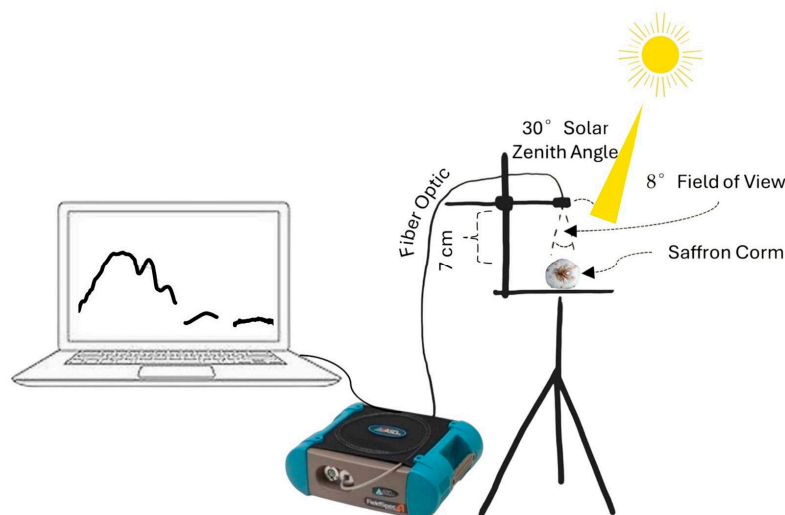


**Figure 2.** Saffron corm spectral measurement setup using the ASD FieldSpec-4 spectrometer with an 8° field of view lens under natural light conditions.

Subsequently, the corms were placed in an oven at 60 °C for one week to achieve complete drying for starch determination. The corms were then reweighed and ground into a fine powder. After that, spectral measurements were performed on the resulting samples to investigate the relationship between the spectral characteristics of the corms and their starch content. This step aimed to evaluate the potential of spectrophotometry as a minimally invasive method for estimating starch content in saffron corms.

#### 2.4. Spectral Data Pre-Processing

Due to outdoor measurement conditions and the presence of atmospheric water vapor, high noise was exhibited in the spectral data in the 1350–1450 nm and 1750–2500 nm regions. These wavelength ranges were consequently masked during data analysis, resulting in 1300 spectral bands being retained for subsequent processing and model development.

Four pre-processing methods, including smoothing with a Savitzky–Golay (SG) filter (frame size of 11 data points, second-degree polynomial), standard normal variate (SNV), multiplicative scatter correction (MSC), and first-derivative (FD) transformations, were applied to reflectance spectra. The mean of three scans for each saffron corm was calculated and used for further processing.

#### 2.5. Feature Engineering: Narrow-Band Ratio Indices

Pearson correlation coefficients were computed between reflectance values at each wavelength and reference measurements for starch and moisture content. Negative correlations were observed between certain spectral bands and starch content, specifically in the overtone and combination bands of C–H and O–H stretches. These bands are known to be related to the presence of starch in plant tissues.

Moreover, the narrow-band hyperspectral indices were computed using the ratio index (RI) to determine the optimal band pairs related to estimating saffron corm starch and moisture content, as defined in Equation (1).

$$RI = \frac{\rho_{\lambda 1}}{\rho_{\lambda 2}} \quad (1)$$

where  $\rho$  and  $\lambda$  are the reflectance and the wavelengths, respectively. For this purpose, all possible two-band combinations were computed after the images' pre-treatment for ASD (1300 bands, 1,690,000 indices). The coefficient of determination ( $R^2$ ) was then cal-

culated for each two-band combination between the derived indices and the starch and moisture content.

### 2.6. Machine Learning Techniques for Moisture and Starch Estimating

To predict starch and water content, partial least squares regression (PLSR), Random Forest (RF), Support Vector Regression (SVR), and Gaussian process regression (GPR) algorithms were applied to the VNIR spectra of fresh corms. The number of latent variables for the PLSR model was optimized using cross-validation to avoid overfitting.

Gaussian process regression (GPR): GPR is a versatile and supervised method for modeling intricate relationships in data and generating forecasts with associated uncertainty. It produces a distribution of all possible functions given the training points, rather than a single function. The GPR method is one of the up-to-date regression techniques and has attracted attention due to its ability to obtain a wide variety of system behavior through covariance functions [29].

Support Vector Regression (SVR): SVR is a powerful regression analysis that has proven to be particularly operational in managing dimensionality when datasets are limited [30]. SVR is a non-linear regression method with low computation costs and relatively high accuracy, founded on the premise of structural risk minimization and statistical learning theory [31].

Partial least squares regression (PLSR): The PLSR technique [32,33] is a proper method for escaping the collinearity across bands problem presented in hyperspectral data [33]. PLSR is a covariance-based strategy that tries to optimize both the explained variance and the correlation between the response variables [34].

Random Forest (RF): The RF technique [35] is an ensemble classifier that employs many decision trees and combines their results to forecast an output. There are two main steps in building each decision tree in an RF: (1) creation of a new training set by random selection of subsamples through bootstrap sampling from a specific number of samples in the original dataset, and (2) random selection of features. These two random processes help to avoid overfitting [36]. The number of trees is obtained using out-of-bag data analysis, and the number of features is obtained using the square root of the features.

The grid search method was used to tune the hyperparameters of the machine learning algorithms. The performance of all possible combinations was assessed using 10-fold cross-validation metrics, and the set of hyperparameters that maximized the average value in cross-validation was selected as the optimal one for training the model (Table 1).

**Table 1.** Hyperparameter tuning process for PLSR, GPR, SVR, and RF algorithms.

PLSR	Parameter	Number of Components			
	Range	1–30			
GPR	Parameter	Basis Function	Kernel Scale	Kernel Function	
	Range	Zero, Constant and Linear	0.001–1000	Exponential, Matern32 and Matern52	
SVR	Parameter	Gamma	C	Kernel Type	
	Range	0.001–100	0.001–100	Gaussian, Linear, Quadratic and Cubic, RBF	
RF	Parameter	N. Learning Cycles	Method	MaxNumSplits	Minimum Leaf Size
	Range	10–500	Bag, LSBoost	1–50	1–50

### 2.7. Model Validation and Performance Metrics

To confirm the models' accuracy, the dataset was divided into 65% (i.e., 85 samples) for training and 35% (i.e., 45 samples) for validation. The model performance was evaluated

using the  $R^2$ , root mean square error (RMSE), residual predictive deviation (RPD), and ratio of performance to interquartile range (RPIQ), as calculated by Equations (2)–(5).

$$R^2 = \frac{\sum_{i=1}^n (\hat{x}_i - \bar{x})^2}{\sum_{i=1}^n (x_i - \bar{x})^2} \quad (2)$$

$$\text{RMSE} = \sqrt{\frac{\sum_{i=1}^n (\hat{x}_i - x)^2}{n}} \quad (3)$$

$$\text{RPD} = \frac{\text{Standard Deviation}}{\text{RMSE}} \quad (4)$$

$$\text{RPIQ} = \frac{\text{IQ}}{\text{RMSE}} \quad (5)$$

where  $x$ ,  $\hat{x}$ , and  $\bar{x}$  represent the measured, predicted, and average observed values, respectively, over  $n$  measurements. The IQ is the interquartile range of the data.

The data handling, spectral pre-processing, and model development (PLSR, RF, SVR, and GPR) were performed in MATLAB 2024b (MathWorks, Natick, MA, USA) using custom-written scripts.

### 3. Results

#### 3.1. Starch and Moisture Content in Saffron Corms

As shown in Table 2, the average starch content in the corms (on a dry-weight basis) was 558 mg g<sup>-1</sup> for the training subset ( $n = 85$ ) and 556 mg g<sup>-1</sup> for the validation subset ( $n = 45$ ). The average moisture contents, based on fresh weight, were 63.1% and 62.8%, respectively, representing the percentage of moisture relative to the total weight of the corms.

**Table 2.** Descriptive statistics for starch and moisture content in saffron corms for training and validation subsets.

Property		N. Sample	Min	Mean	Max	Standard Deviation
Starch Content (mg g <sup>-1</sup> )	Training	85	428	558	701	60.6
	Validation	45	452	556	698	58.2
Moisture Content (%)	Training	85	50.3	63.1	70.2	3.49
	Validation	45	54.2	62.8	69.8	3.62

#### 3.2. Spectral Characteristics of Saffron Corm

Over 350–2350 nm, the reflectance spectra of fresh and dried, powdered saffron corms displayed three distinct profiles with instrumental gaps at ~1350–1450 nm and ~1750–1900 nm (visible as blank intervals), as shown in Figure 3. Although a characteristic absorption feature related to starch is present around ~2100 nm, this spectral region is included only for visual comparison of spectral characteristics in Figure 3 and was not considered in the modeling process. Consequently, wavelengths beyond 1750 nm were excluded from further analysis.

For fresh corms, the spectral profile was dominated by strong water absorption features. Reflectance rose from ~0.1–0.25 at 400 nm to a broad maximum (~0.6–0.7) in the near-infrared range (700–900 nm), with characteristic dips associated with water (e.g., ~970 nm, ~1200 nm) and broad overtone bands of organic constituents (Figure 3a).

In contrast, the spectra of dried, powdered corms showed significantly higher reflectance (Figure 3b). In the VNIR region (400–1350 nm), reflectance rose from ~0.05–0.15 at

400 nm to a broad maximum of  $\sim 0.95$  near  $\sim 1000$  nm, with minor variations in reflectance. A pronounced downturn occurs between  $\sim 1100$ – $1250$  nm, followed by a secondary rise toward  $\sim 1350$  nm. In the first SWIR window (1450–1750 nm), spectra lie around  $\sim 0.40$ – $0.60$  and show a broad hill centered near  $\sim 1600$  nm with shoulders at  $\sim 1500$ – $1550$  nm and  $\sim 1680$ – $1710$  nm. In the second SWIR window (1900–2350 nm), reflectance is lower ( $\sim 0.12$ – $0.30$ ) and exhibits two repeatable feature sets: (i) peak–troughs around  $\sim 2000$ – $2100$  nm and (ii) structured bands over  $\sim 2150$ – $2300$  nm. Across all windows, similar line-shape patterns are shown; variability appears primarily as vertical intensity offsets rather than wavelength shifts, and the deep minima typical of strong water bands are notably attenuated in these dried powders.

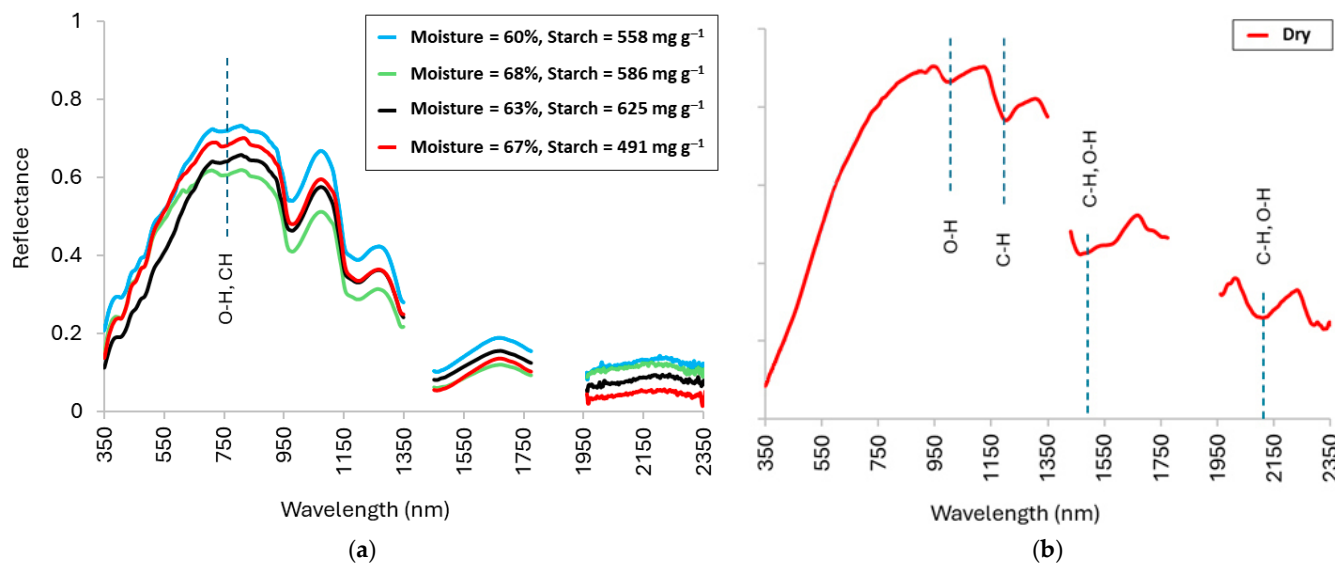


**Figure 3.** Reflectance spectra of (a) wet saffron corms with different moisture and starch contents (each line = one corm; spectrum averaged over 3 scans) shown as examples with their corresponding reference water (%) and starch ( $\text{mg g}^{-1}$ , dry weight) and (b) dried (average of 12 samples), powdered saffron corms over 350–2350 nm showing a steep rise to  $\sim 1000$  nm, a downturn at 1100–1250 nm, a broad hill near 1600 nm, and structured bands at 2000–2100 and 2150–2300 nm (instrumental gaps at  $\sim 1350$ – $1450$  and  $1750$ – $1900$  nm).

### 3.3. Wavelength-Specific Correlation with Starch and Moisture

Pearson’s wavelength-dependent correlation analysis revealed weak but consistent trends with starch and moisture content in fresh corms (Figure 4). Water content showed uniformly negative correlations across the recorded range. Coefficients decreased smoothly to about  $-0.05$  over 500–800 nm, reached a local minimum at  $\sim 930$ – $1000$  nm ( $\approx -0.10$ ), exhibited a shallow shoulder at  $\sim 1030$ – $1070$  nm ( $\approx -0.06$  to  $-0.07$ ), and declined again over 1150–1220 nm ( $\approx -0.12$  to  $-0.13$ ). The deepest minimum occurred around 1300–1350 nm ( $\approx -0.15$  to  $-0.16$ ). After the spectral gap ( $\sim 1350$ – $1450$  nm), correlations remained consistently negative at  $\sim -0.10 \pm 0.01$  through 1450–1750 nm. Collectively, the dataset delineates three water-informative windows:  $\sim 930$ – $1000$  nm, 1150–1220 nm, and 1270–1330 nm.

Starch content exhibited a different pattern, with predominantly positive correlations in the visible-to-short-wave NIR region (400–900 nm, from  $\sim +0.09$  down toward zero), with modest positive undulations over 950–1250 nm ( $\approx 0$  to  $+0.02$ ). In the post-gap region (1450–1750 nm), coefficients were mildly negative ( $\approx -0.04$ ) and showed a trend toward zero. The discontinuity between  $\sim 1350$  and 1450 nm reflects a missing spectral segment in the input data.

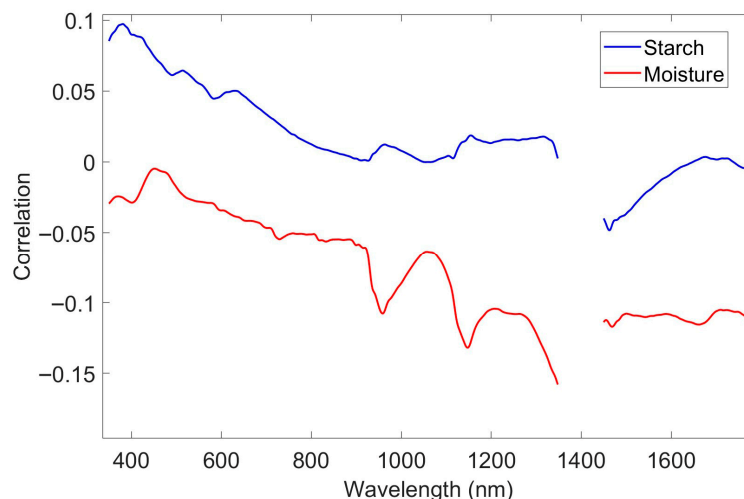


**Figure 4.** Pearson correlation ( $r$ ) versus wavelength between VNIR reflectance and composition in fresh saffron corms ( $n = 130$ ): moisture (red) is uniformly negative; starch (blue) is generally positive. The 1350–1450 nm gap indicates missing data.

### 3.4. Optimal Narrow-Band Spectral Indices

The predictive power of all possible two-band ratio indices (RIs) was mapped using  $R^2$  heatmaps (Figure 5). For moisture, the highest  $R^2$  values exhibited an intense, elongated region along the main diagonal centered at 930–1000 nm and 1050–1150 nm, accompanied by an elongated band of elevated correlation over ~1300–1350 nm. Additionally, fluctuations in moisture content were observed at wavelengths below 800 nm. For starch, the most predictive region was more limited, centered in the ~730–900 nm range with a narrow ridge along the diagonal at ~740–930 nm. Only weak, isolated peaks are present near ~400–520 nm and ~1000–1100 nm. Above 1300 nm, additional weak features were observed, but they were poorly resolved due to the masked spectral gaps (1350–1450 and 1750–1900 nm). The optimal band pairs and their performance are summarized in Table 3. For water content, the best-performing band pair was RI ( $\lambda_{1182}$ ,  $\lambda_{1305}$ ), with a modest  $R^2 = 0.41$  and RMSE = 2.82%. For starch, the highest performance was obtained with RI ( $\lambda_{735}$ ,  $\lambda_{810}$ ), with  $R^2 = 0.35$  and RMSE = 43.1 mg  $g^{-1}$ . Overall, these two-band indices show limited predictive potential. The corresponding calibration equations are provided in Table 3.

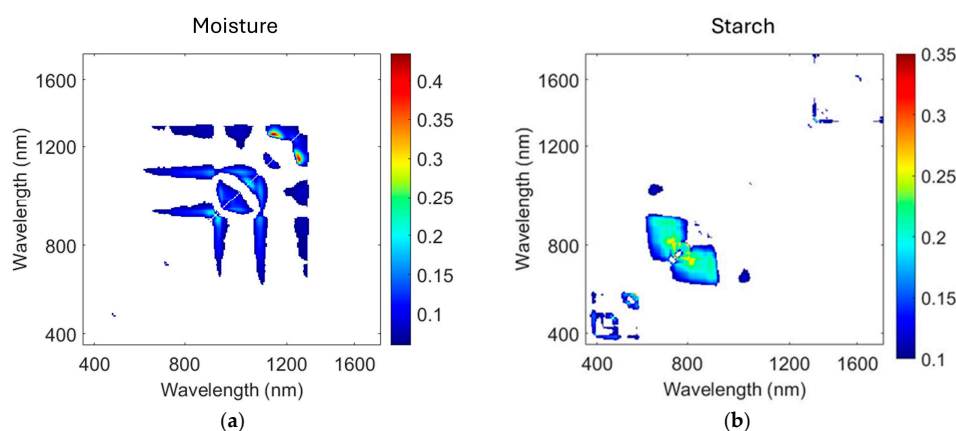


**Figure 5.** Two-dimensional  $R^2$  heat maps of RI narrow-band spectral indices (based on wavelength-pair combinations) for estimating (a) water content and (b) starch content from reflectance spectra (400–1750 nm). Warmer colors indicate higher  $R^2$ . Water shows the strongest structure in ~900–1350 nm (maximum around 1.20–1.26  $\mu\text{m}$ ), while starch exhibits compact, high- $R^2$  blocks in the ~730–900 nm range; the sparse band at 1350–1450 nm reflects a measurement gap.

**Table 3.** Optimal narrow-band ratio index (RI) for predicting starch and moisture content in saffron corms.

Optimal Band Pair	R <sup>2</sup>	RMSE	Equation
RI (λ <sub>1182</sub> , λ <sub>1305</sub> )	0.41	2.82	Water (%) = 323 × $\frac{\rho_{\lambda_{1182}}}{\rho_{\lambda_{1305}}}$ - 267
RI (λ <sub>735</sub> , λ <sub>810</sub> )	0.35	43.1	Starch (mg g <sup>-1</sup> ) = 635 × $\frac{\rho_{\lambda_{735}}}{\rho_{\lambda_{810}}}$ + 1.2

3.5. Predictive Performance for Starch and Water Content Estimation

The performance of the PLSR, RF, SVR, and GPR algorithms to estimate the saffron corm starch and water content using VNIR spectra pre-processed by SG, SNV, MSC, and FD is reported in Table 4. The results showed that the moisture content was predicted with higher accuracy than starch content across all ML algorithms and pre-processing methods, while starch content prediction was moderately successful.

**Table 4.** Comparative performance of PLSR, RF, SVR, and GPR models in predicting starch and moisture content in saffron corms using VNIR spectra pre-processed by SG, SNV, MSC, and FD (n = 45).

Property	Algorithm	Pre-Processing	R <sup>2</sup>	RMSE	RPD	RPIQ
Starch	GPR	SG	0.61	36.7	1.76	2.37
		SNV	0.68	33.7	1.92	2.59
		MSC	0.70	30.4	2.01	2.66
		FD	0.70	37.1	1.99	2.73
	SVR	SG	0.58	38.2	1.69	2.45
		SNV	0.60	31.8	1.96	2.85
		MSC	0.65	35.5	1.91	2.42
		FD	0.65	36.3	1.85	2.17
	PLSR	SG	0.64	34.0	1.85	2.32
		SNV	0.69	29.7	2.03	2.31
		MSC	0.73	28.7	2.14	2.81
		FD	0.67	36.6	1.92	2.64
	RF	SG	0.59	37.5	1.69	2.30
		SNV	0.69	30.1	2.07	2.77
		MSC	0.71	32.3	2.00	2.54
		FD	0.65	37.2	1.87	2.97
Moisture Content	GPR	SG	0.88	1.00	2.87	4.20
		SNV	0.91	0.88	3.93	4.79
		MSC	0.92	0.71	4.56	5.37
		FD	0.88	0.99	3.48	4.19
	SVR	SG	0.79	1.33	2.47	3.36
		SNV	0.82	1.28	2.90	3.80
		MSC	0.85	1.15	2.99	4.62
		FD	0.81	1.33	2.68	2.66
	PLSR	SG	0.88	0.99	3.18	4.00
		SNV	0.89	0.97	3.65	5.20
		MSC	0.92	0.81	4.21	5.27
		FD	0.89	0.93	3.60	3.67
	RF	SG	0.80	1.24	2.71	3.38
		SNV	0.83	1.31	2.77	3.71
		MSC	0.84	1.19	2.91	3.64
		FD	0.82	1.26	2.81	2.93

Among the various models evaluated for starch, PLSR in combination with MSC pre-processing yielded the best results, achieving the highest  $R^2$  value (0.73), RPD (2.14), and RPIQ (2.81), as well as the lowest RMSE (28.7). Except for SVR, all other algorithms (i.e., PLSR, GPR, and RF) exhibited RPD values higher than 2 and an RPIQ higher than 2.5 for starch estimation using MSC pre-processing.

For moisture content prediction, the GPR model in combination with MSC pre-processing yielded the best results, with an  $R^2$  value of 0.92, RPD value of 4.56, and RPIQ value of 5.37, as well as the lowest RMSE (0.71). The PLSR-MSC combination ranked second in performance after GPR-MSC. Across all pre-processing methods, SVR and RF exhibited RPD values lower than 3 and RPIQ values higher than 4 for corm moisture estimation.

Figures 6a and 6b show scatter plots of measured versus estimated values for moisture content and starch of saffron corms, respectively, obtained using the PLSR, RF, SVR, and GPR algorithms coupled with SG, SNV, MSC, and FD pre-processing methods.

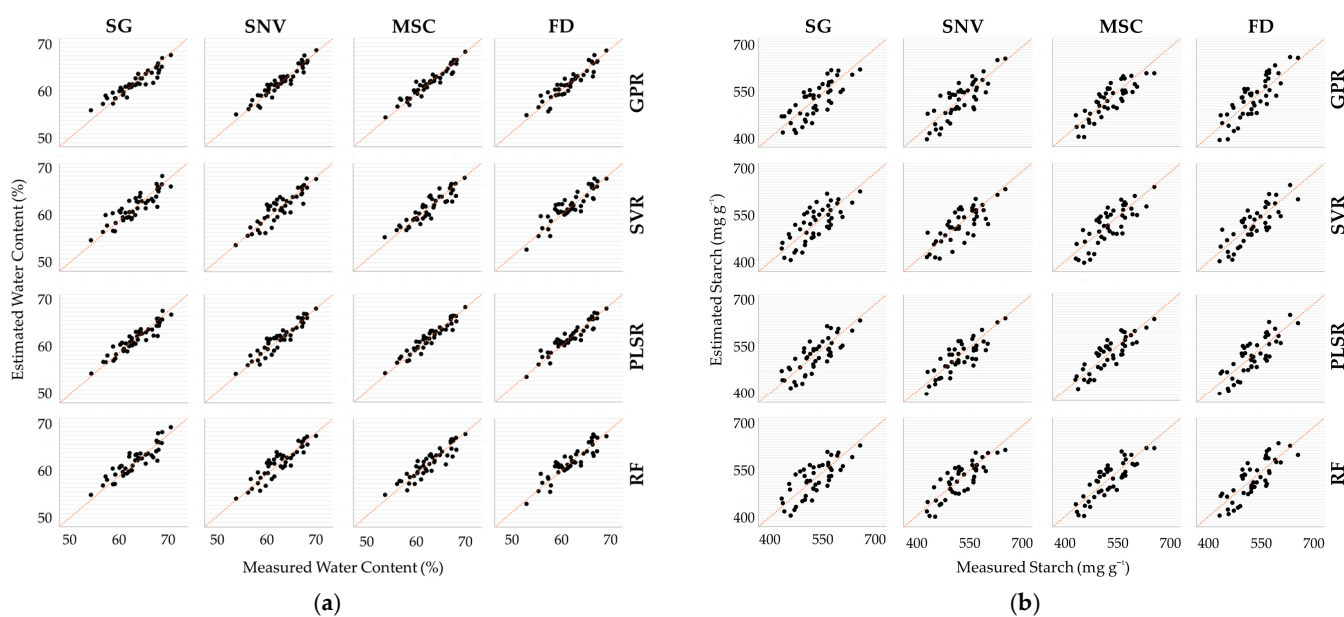


**Figure 6.** Measured vs. predicted plots ( $n = 45$ ) for (a) moisture content and (b) starch content in fresh saffron corms using VNIR spectroscopy. Rows represent different machine learning algorithms (PLSR, GPR, SVR and RF), and columns represent different pre-processing methods (SG, SNV, MSC and FD).

For corm moisture content, data points clustered tightly along the 1:1 line with no evident systematic bias for neither the ML algorithms nor pre-processing methods. Dispersion remains nearly uniform across the domain, indicating stable precision over low-to high-moisture samples (Figure 6a). Figure 6a shows scatter plots of measured versus estimated moisture content for all model–pre-processing combinations, with the diagonal 1:1 line indicating perfect agreement. The GPR-MSC scatter plot exhibits the tightest clustering of points around the diagonal across the entire measured range (50–70%), with no apparent systematic bias. PLSR-MSC and GPR-SNV also show good point alignment, though with slightly greater dispersion. In contrast, RF-based models display wider scatter and frequent deviations from the 1:1 line, particularly at the extremes of the moisture range. SVR-MSC shows moderate clustering but with some overestimation at low moisture values and underestimation at high values. These visual patterns corroborate the quantitative metrics ( $R^2$ , RPD, RMSE) reported in Table 4, confirming that GPR-MSC and PLSR-MSC provide the most accurate moisture content predictions.

Figure 6b presents scatter plots of measured versus estimated starch content in saffron corms for the PLSR, RF, SVR, and GPR algorithms coupled with SG, SNV, MSC, and FD pre-processing methods. Each subplot shows the measured starch content ( $x$ -axis, ranging from approximately 400 to 700  $\text{mg}\cdot\text{g}^{-1}$  dry weight) plotted against the corresponding estimated values ( $y$ -axis), with the diagonal 1:1 line representing perfect agreement. For the PLSR-MSR combination, which achieved the best predictive performance ( $R^2 = 0.73$ ,  $\text{RPD} = 2.14$ ,  $\text{RPIQ} = 2.81$ ), the data points cluster reasonably well around the diagonal line, although greater dispersion is observed compared to the moisture content scatter plots. Some overestimation occurs at lower starch values (approximately 400–450  $\text{mg}\cdot\text{g}^{-1}$ ), and slight underestimation is evident at higher values (above 650  $\text{mg}\cdot\text{g}^{-1}$ ). GPR with MSR or FD pre-processing shows moderate clustering around the 1:1 line, with  $\text{RPD}$  values of approximately 2.0, indicating acceptable predictive accuracy. SVR-based models exhibit wider point dispersion and more frequent deviations from the diagonal, consistent with their lower  $\text{RPD}$  values (1.69–1.96). RF models show intermediate performance, with  $\text{RPD}$  values ranging from 1.69 to 2.07. Overall, the scatter plots visually confirm that PLSR-MSR provides the most accurate starch content estimates among the models evaluated, though with greater uncertainty than observed for moisture content prediction, reflecting the more challenging nature of starch quantification using VNIR spectroscopy.

## 4. Discussion

### 4.1. Interpretation of Starch and Moisture Content in Saffron Corms

On a dry-weight basis, the average starch content in saffron corms was approximately 558  $\text{mg}\cdot\text{g}^{-1}$  (Table 2), indicating a significant amount of this compound in the corm tissue. Starch plays an important role in the plant's metabolic processes, including flowering and energy storage. The role of starch content as a key factor in corm growth and daughter corm formation has been recently documented [37]. Additionally, the moisture content of the corms was 63% (Table 2) on a fresh-weight basis, reflecting a high level of moisture in the plant tissue. High moisture content may be crucial in maintaining cell density and protecting against environmental stresses during the early growth stages [38]. Compared with the active growth phase of the plant, mid-to-late summer (around August) coincides with the dormant period of saffron corms, during which above-ground growth ceases and physiological activity is minimal. During this period, the corms neither absorb water nor retain water in their tissues. Mid- and late summer may represent a favorable period for spectroscopic measurement (starch), as the moisture content, which can interfere with the accurate prediction of starch content, is at its lowest [37]. Together, starch and moisture content represent critical physiological factors that determine the saffron's quality and health, as well as its subsequent flowering potential.

### 4.2. Spectral Signatures and Their Biochemical Basis

The positive correlation between VNIR reflectance and starch content, particularly pronounced in the 930–1000 nm, 1150–1200 nm, and 1270–1330 nm ranges (Figure 4), aligns with known carbohydrate absorption features. These correlations can be attributed to light scattering resulting from the structural characteristics of starch in these regions. Starch is stored in the plant tissue as semi-crystalline granules, which consist of both amorphous and crystalline layers. This structure is influenced by the ratio of amylose to amylopectin [39]. Additionally, the shape and method of starch storage may affect how the light is reflected. Starch granules may be oval or polyhedral [40] and the way light is reflected from each of these shapes may vary. Similar studies have reported negative correlations for starch within these spectral regions, with the scattering effects being especially significant in amylopectin and amylose and their molecular structure [41,42].

The negative correlation between moisture and reflectance across the 400–900 nm range is more complex and likely indirect. This pattern is more likely consistent with moisture-induced, indirect changes in tissue scattering and overall optical behavior, rather than direct absorption by water. In contrast, in water-sensitive near-infrared regions (approximately 970–1200 nm and around the 1450 nm water absorption band), increased moisture is expected to reduce reflectance, which accords with the slightly negative correlations observed beyond 1450 nm [43]. Therefore, the light absorption characteristics of moisture in these spectral regions may seem logical, as water molecules naturally absorb light. On the other hand, because water molecules contain hydroxyl groups, they can affect signals in the VNIR region. Given that the moisture content in the saffron corm is much higher than that of starch, any wavelength that is more influenced by the moisture content may indirectly show an inverse correlation with the starch content itself. Hydroxyl (O–H) bonds can absorb light and reduce reflectance. Because O–H groups exist in both water and starch, these absorptions may reflect contributions from both. However, since the moisture content of the saffron corm is much higher than the starch content, bands that are sensitive to both moisture and starch are likely dominated by moisture, meaning the apparent starch-related signal may be influenced by moisture. The dominance of the water signal makes it difficult to predict starch content, as water absorption can mask or alter the subtle spectral signatures of starch, which explains the inverse correlation pattern noted in some regions. Given that the water content of saffron corms is at its minimum just before planting, performing spectral measurements at that time is suggested.

#### 4.3. Spectral Profiles of Fresh and Powdered Saffron Corms Across 400–2350 nm

Figure 3 shows the VNIR–SWIR reflectance behavior of fresh (wet) corms and dried, powdered material. Across 400–1350 nm, reflectance increases steeply toward a broad maximum near ~1000 nm, followed by a pronounced downturn over ~1100–1250 nm and partial recovery toward the end of the VNIR window. This behavior is consistent with that typically observed in plant tissue optics, where high NIR reflectance is strongly influenced by internal scattering, while water-related features contribute to localized absorption around the NIR plateau [44,45]. The presence of O–H, C–H, and C–O bonds can lead to light absorption and the creation of vibrational modes in these areas. The absorption feature at 750 nm could be related to the third O–H band and the fourth overtone of C–H [46].

In the SWIR region, reflectance is lower and exhibits a repeatable structure at wavelengths of around 2000–2100 nm and 2150–2300 nm. Earlier studies on dry plant materials have reported features in these intervals. The absorptions of 1200 nm, 1450–1600 nm, and 2100 nm are often linked to overtone and combination bands of O–H and C–H vibrations containing components such as cellulose and starch [47–49]. Two blank intervals, at ~1350–1450 nm and ~1750–1900 nm, correspond to instrumental gaps (missing spectral data) in the acquisition system and were excluded from interpretation. This may be because measurements were made outdoors under natural illumination. Compared to fresh corms, the dried powders are less influenced by liquid water and more influenced by particle-scale scattering. This can reduce the prominence of water-related spectral features and modify the overall reflectance intensity.

#### 4.4. Two-Dimensional $R^2$ Maps of RI Band-Pair Indices: Key Wavelengths for Water and Starch

The two-dimensional  $R^2$  maps for moisture and starch reveal specific regions of the spectrum that exhibit the highest  $R^2$  values for these features. For moisture, the strongest correlations were observed in the 930–1000, 1050–1150 nm, and 1300–1350 nm regions. In line with Table 3, the optimal RI band pair for moisture was  $\lambda_{1182}/\lambda_{1305}$ . These spectral regions are consistent with water-related absorption features in the NIR range. Such

features are usually attributed to O–H bonds in water molecules. So, changes in a sample's water content show up as changes in NIR absorption. In studies on plant materials, these regions have been reported as moisture-sensitive areas. These results show that selected wavelength pairs capture informative moisture-related variation in the NIR range [50,51]. This finding effectively demonstrates that moisture prediction through VNIR spectroscopy can be achieved with the use of useful bands (band-pair selection).

For starch, two-dimensional  $R^2$  maps indicated stronger activity in the 740–930 nm regions. Accordingly, Table 3 identified  $\lambda_{735}/\lambda_{810}$  as the optimal RI band pair for starch. These wavelengths may be related to vibrations of O–H and C–H bonds, which are present in amylose and amylopectin. These areas may reflect the impact of amylopectin and amylose on light scattering, as reported in similar studies [52,53]. The sparse region at 1350–1450 nm reflects the measurement gap in the spectra. However, the correlations in regions above 1000 nm were weaker, which may be linked to lower light scattering and the specific characteristics of starch in these regions. In the wavelength range of 400 to 500 nanometers, where some changes have been observed, no evidence of starch absorption has yet been found. This could be due to the physical and chemical structure of starch or phenomena such as light scattering.

#### 4.5. Machine Learning Algorithm Performance for Starch and Moisture Prediction

The PLSR model achieved the best predictive accuracy for the starch content of saffron corms using VNIR spectra in comparison with other models (RF, SVR, and GPR), yielding an  $R^2$  of 0.73, RMSE of  $28.7 \text{ mg}\cdot\text{g}^{-1}$ , RPD of 2.14, and RPIQ of 2.81 when coupled with MSC pre-processing. For moisture content, GPR-MSR produced the highest accuracy ( $R^2 = 0.92$ , RMSE = 0.71%, RPD = 4.56, RPIQ = 5.37), with PLSR-MSR ranking second ( $R^2 = 0.92$ , RMSE = 0.81%, RPD = 4.21, RPIQ = 5.27). As shown in Figure 6a, the data points for moisture prediction are tightly clustered along the 1:1 line with no evident systematic bias and relatively uniform dispersion, indicating stable prediction precision across low- to high-moisture samples [54].

Compared with moisture, starch prediction showed moderate performance. As shown in Figure 6b, a linear trend is observable across the approximate range of 400–750  $\text{mg}\cdot\text{g}^{-1}$ , yet greater scatter and slight underestimation at higher starch concentrations (above approximately 600  $\text{mg}\cdot\text{g}^{-1}$ ) are evident. This reduced accuracy can be attributed to three main factors: first, the overwhelming spectral influence of water, which complicates the detection of the weaker starch signal; second, the light-scattering properties of semi-crystalline starch granules, which are influenced by granule size, shape, and the amylose-to-amylopectin ratio [40,41]; and third, potential non-linear interactions between water and starch in the fresh tissue matrix. The moderate performance suggests that while VNIR spectroscopy can rank corms by starch content, its use for precise quantitative determination may require enhanced calibration strategies; for instance, neural network models have shown benefits in similar applications [55,56].

Given that evaluations of global saffron germplasms have confirmed homogeneous genotypes worldwide [57], the minor variation in moisture and starch content of corms from different batches, attributable to geographic and climatic conditions as well as management practices, can be considered minimal. These minor variations are unlikely to substantially affect model performance, although recalibration with additional diverse samples would further enhance accuracy.

#### 4.6. Spectral Pre-Processing Performance for Starch and Moisture Prediction

Based on the results reported in Table 4, MSR was the best pre-processing method when coupled with most machine learning algorithms for both starch and water content

prediction. Following MSC, SNV and FD transformations also demonstrated high capability, yielding competitive predictive accuracy across multiple models. In contrast, SG smoothing resulted in lower accuracy compared to the other pre-processing methods in most cases. Given that measurements were conducted under natural light with considerable fluctuations in illumination conditions, this outcome is sensible. MSC and SNV are both designed to correct for scattering effects caused by particle size heterogeneity and variable light paths, which are common when measuring intact corms under non-laboratory illumination. FD transformation effectively removes baseline shifts and enhances spectral resolution, which may explain its strong performance despite the absence of explicit scatter correction. The relatively poor performance of SG smoothing suggests that simple noise reduction is insufficient when scattering effects dominate the spectral variability. These findings highlight the importance of selecting scatter-correcting pre-processing methods (MSC or SNV) when developing robust predictive models for corm quality attributes under variable measurement conditions.

#### 4.7. Limitations and Future Work

The present study was conducted on a single kind of saffron corm. To provide a general model, it is suggested that future studies consider corms grown in different geographic and climatic conditions, which could possibly have genetic differences. This study proves the capability of VNIR spectroscopy for assessing saffron corm status.

For on-farm applicability in future work, designing a portable instrument with internal illumination that can perform spectral measurements of corms through a small perforation in the corm tunic without requiring their removal is needed.

Moreover, with respect to the important role of moisture in masking spectral reflectance informativity and the fluctuation of water content levels in corms over time, future research could focus on methods like external parameter orthogonalization (EPO) to account for the effect of water content and better study the corms' status.

## 5. Conclusions

This study demonstrates that VNIR spectroscopy is an effective, minimally invasive method for the rapid assessment of key compositional traits in saffron corms. Among the evaluated models (PLSR, RF, SVR, and GPR), PLSR provided the best predictive performance for both traits. Moisture content was predicted with strong accuracy ( $R^2 = 0.89$ , RMSE = 0.91%, RPD = 3.67, RPIQ = 4.91), while starch content achieved moderate but informative precision ( $R^2 = 0.68$ , RMSE = 26.29 mg g<sup>-1</sup>, RPD = 1.87, RPIQ = 2.37, dry basis). Wavelength-dependent analysis identified starch-sensitive intervals (~930–1000 nm and ~1150–1220 nm) and confirmed the strong influence of moisture in the 900–1350 nm range. The results confirm the potential of laboratory-based VNIR spectroscopy as a research tool for evaluating pre-planting corms under controlled conditions. The method offers a scientifically grounded approach complementary to destructive laboratory analyses, enabling the assessment of moisture in saffron corms and providing a basis for starch estimation that requires further validation for field applications. This leads to the grading and selection of corms based on their physiological reserves. To enhance robustness and transition toward field application, field validation with portable, cost-effective spectrometers under real farm conditions should be prioritized to demonstrate practical deployment feasibility. Future work should also evaluate the use of controlled illumination and purpose-specific wavelength selection, as well as alternative sensing modes such as interactance or transmittance, which may better capture internal corm properties than surface reflectance alone.

**Author Contributions:** Conceptualization, S.M. (Saham Mirzaei) and R.R.; Methodology, S.M. (Saham Mirzaei), M.F., F.S., A.S., M.C., S.M. (Shahriar Mahdavi) and A.N.; Software, M.F. and S.M. (Saham

Mirzaei); Investigation, M.F. and A.P.; Resources, R.R. and F.O.; Data curation, M.F.; Writing—original draft preparation, M.F.; Writing—review and editing, all authors; Supervision, R.R., G.P. and F.S. All authors have read and agreed to the published version of the manuscript.

**Funding:** This research received no external funding.

**Data Availability Statement:** The datasets generated and analyzed during the current study are available from the corresponding author on reasonable request.

**Acknowledgments:** The authors acknowledge the Institute of Methodologies for Environmental Analysis of the Italian National Research Council for providing spectroscopy facilities.

**Conflicts of Interest:** The authors declare no conflicts of interest.

## Abbreviations

The following abbreviations are used in this manuscript:

AMG	Amyloglucosidase
FD	First Derivative
GC	Gas Chromatography
GPR	Gaussian Process Regression
GOPOD	Glucose Oxidase/Peroxidase
HPLC	High-Performance Liquid Chromatography
MSC	Multiplicative Scatter Correction
PLSR	Partial Least Squares Regression
RPD	Residual Predictive Deviation
RPIQ	Ratio of Performance to Interquartile Range
RMSE	Root Mean Square Error
RTS	Rapid Total Starch
SG	Savitzky–Golay
SWIR	Short-Wave Infrared
SNV	Standard Normal Variate
SVR	Support Vector Regression
RF	Random Forest
VNIR	Visible and Near-Infrared

## References

- Cardone, L.; Castronuovo, D.; Perniola, M.; Cicco, N.; Candido, V. Saffron (*Crocus sativus* L.), the King of Spices: An Overview. *Sci. Hortic.* **2020**, *272*, 109560. [[CrossRef](#)]
- Avila-Sosa, R.; Nevárez-Moorillón, G.V.; Ochoa-Velasco, C.E.; Navarro-Cruz, A.R.; Hernández-Carranza, P.; Cid-Pérez, T.S. Detection of Saffron's Main Bioactive Compounds and Their Relationship with Commercial Quality. *Foods* **2022**, *11*, 3245. [[CrossRef](#)] [[PubMed](#)]
- Cardone, L.; Candido, V.; Castronuovo, D.; Perniola, M.; Cicco, N. Comparing Annual and Biennial Crop Cycle on the Growth, Yield and Quality of Saffron Using Three Corm Dimensions. *Sci. Hortic.* **2021**, *288*, 110393. [[CrossRef](#)]
- Naseri, E.; Dalir, N.; Mokhtassi-Bidgoli, A.; Ebadi, M.T.; Rahnemaie, R. Optimizing Saffron Cormlet Production through Substrate Composition Nutrient Concentration and Irrigation Management in Soilless Cultivation. *Sci. Rep.* **2025**, *15*, 36. [[CrossRef](#)]
- Dewir, Y.H.; Alsadon, A.; Ibrahim, A.; El-Mahrouk, M. Effects of Growing Substrate, Mode of Nutrient Supply, and Saffron Corm Size on Flowering, Growth, Photosynthetic Competence, and Cormlet Formation in Hydroponics. *Horttechnology* **2022**, *32*, 234–240. [[CrossRef](#)]
- Ralli, P.E.; Menexes, G.; Dordas, C.A. Corm Size and Planting Density Affect the Yield and Longevity of Saffron (*Crocus sativus* L.). *Not. Bot. Horti Agrobot. Cluj Napoca* **2024**, *52*, 13556. [[CrossRef](#)]
- Chrungoo, N.K.; Farooq, S. Correlative Changes in Carbohydrate Content and Starch Hydrolysing Enzymes in Corms of Saffron *Crocus* (*Crocus sativus* L.) during Dormancy and Sprouting. *Biochem. Physiol. Pflanz.* **1985**, *180*, 55–61. [[CrossRef](#)]
- Kamenetsky, R.; Zemah, H.; Ranwala, A.P.; Vergeldt, F.; Ranwala, N.K.; Miller, W.B.; Van As, H.; Bendel, P. Water Status and Carbohydrate Pools in Tulip Bulbs during Dormancy Release. *New Phytol.* **2003**, *158*, 109–118. [[CrossRef](#)]

9. Bagri, J.; Yadav, A.; Anwar, K.; Dkhar, J.; Singla-Pareek, S.L.; Pareek, A. Metabolic Shift in Sugars and Amino Acids Regulates Sprouting in Saffron Corm. *Sci. Rep.* **2017**, *7*, 11904. [[CrossRef](#)]
10. Renau-Morata, B.; Nebauer, S.G.; Sánchez, M.; Molina, R.V. Effect of Corm Size, Water Stress and Cultivation Conditions on Photosynthesis and Biomass Partitioning during the Vegetative Growth of Saffron (*Crocus sativus* L.). *Ind. Crops Prod.* **2012**, *39*, 40–46. [[CrossRef](#)]
11. Koocheki, A.; Khajeh-Hosseini, M. *Saffron: Science, Technology and Health*; Woodhead Publishing: Duxford, UK, 2020.
12. Yang, W.; Li, X.; Chang, F.; Qiu, X.; Huang, X.; Feng, Z.; Yan, J.; Wu, Q.; Wen, F.; Pei, J.; et al. Low light reduces saffron corm yield by inhibiting starch synthesis. *Front. Plant Sci.* **2025**, *16*, 1544054. [[CrossRef](#)]
13. Maleki, F.; Kazemi, H.; Siahmarguee, A.; Kamkar, B. Development of a Land Use Suitability Model for Saffron (*Crocus sativus* L.) Cultivation by Multi-Criteria Evaluation and Spatial Analysis. *Ecol. Eng.* **2017**, *106*, 140–153. [[CrossRef](#)]
14. Acharya, B.S.; Ghalegholabbehbahani, A.; Hamido, S.; Zinati, G.; Bozzolo, A.; Archer, L.; Wendelberger, K.; Das, S.; Thapa, R.; Panday, D. Saffron (*Crocus sativus* L.): The Golden Spice—Management, Challenges, and Opportunities for Sustainable Production in the United States. *J. Agric. Food Res.* **2025**, *21*, 101970. [[CrossRef](#)]
15. Ziaei, S.M.; Feizi, H.; Siuki, A.K.; Sahabi, H. Yield and Quality of Saffron (*Crocus sativus* L.) in Response to Priming Treatments and Water Deficit. *Ital. J. Agron.* **2024**, *19*, 100020. [[CrossRef](#)]
16. Mena-García, A.; Sanz, M.L.; Díez-Municio, M.; Ruiz-Matute, A.I. A Combined Gas and Liquid Chromatographic Approach for Quality Evaluation of Saffron-Based Food Supplements. *Foods* **2023**, *12*, 4071. [[CrossRef](#)]
17. Eghbali, S.; Farhadi, F.; Askari, V.R. An Overview of Analytical Methods Employed for Quality Assessment of *Crocus sativus* (Saffron). *Food Chem. X* **2023**, *20*, 100992. [[CrossRef](#)] [[PubMed](#)]
18. Jantra, C.; Slaughter, D.C.; Liang, P.-S.; Pathaveerat, S. Nondestructive Determination of Dry Matter and Soluble Solids Content in Dehydrator Onions and Garlic Using a Handheld Visible and Near Infrared Instrument. *Postharvest Biol. Technol.* **2017**, *133*, 98–103. [[CrossRef](#)]
19. Ricci, C.; Gadaleta, A.; Gerardino, A.; Didonna, A.; Ferrara, G.; Bertani, F.R. Portable optical spectroscopy and machine learning techniques for quantification of the biochemical content of raw food materials. *CABI Agric. Biosci.* **2024**, *5*, 39. [[CrossRef](#)]
20. Angel Prieto Lage, M.; Barral Martínez, M.; Seyyedimansour, S.; Manikantan, M.R.; Trif, M.; Khaneghah, M.A. Recent Advancements in NIR Spectroscopy for Assessing the Quality and Safety of Horticultural Products: A Comprehensive Review. *Front. Nutr.* **2022**, *9*, 973457. [[CrossRef](#)]
21. Fodor, M.; Matkovits, A.; Benes, E.L.; Jókai, Z. The Role of Near-Infrared Spectroscopy in Food Quality Assurance: A Review of the Past Two Decades. *Foods* **2024**, *13*, 3501. [[CrossRef](#)]
22. Darvishi Bolorani, A.; Mirzaei, S.; Bahrami, H.A.; Soleimani, M.; Neysani Samany, N.; Papi, R.; Mahmoudi, M.; Bakhtiari, M.; Huete, A. In vitro plant spectral response reveals dust stress. *Agric. For. Meteorol.* **2025**, *370*, 110599. [[CrossRef](#)]
23. Darvishi Bolorani, A.; Ranjbar, S.; Mirzaei, S.; Bahrami, H.A.; Mirzapour, F.; Abbaszadeh Tehrani, N. Spectral behavior of Persian oak under compound stress of water deficit and dust storm. *Int. J. Appl. Earth Obs. Geoinf.* **2020**, *88*, 102082. [[CrossRef](#)]
24. Rawal, A.; Hartemink, A.; Zhang, Y.; Wang, Y.; Lankau, R.A.; Ruark, M.D. Visible and Near-Infrared Spectroscopy Predicted Leaf Nitrogen Contents of Potato Varieties under Different Growth and Management Conditions. *Precis. Agric.* **2024**, *25*, 751–770. [[CrossRef](#)]
25. Bai, S.H.; Tootoonchy, M.; Kämper, W.; Tahmasbian, I.; Farrar, M.B.; Boldingh, H.; Pereira, T.; Jonson, H.; Nichols, J.; Wallace, H.M.; et al. Predicting Carbohydrate Concentrations in Avocado and Macadamia Leaves Using Hyperspectral Imaging with Partial Least Squares Regressions and Artificial Neural Networks. *Remote Sens.* **2024**, *16*, 3389. [[CrossRef](#)]
26. Wang, Z.; Li, J.; Zhang, C.; Fan, S. Development of a General Prediction Model of Moisture Content in Maize Seeds Based on LW-NIR Hyperspectral Imaging. *Agriculture* **2023**, *13*, 359. [[CrossRef](#)]
27. Alighaleh, P.; Pakdel, R.; Ghanei Ghooshkhaneh, N.; Einafshar, S.; Rohani, A.; Saeidirad, M.H. Detection and Classification of Saffron Adulterants by Vis-Nir Imaging, Chemical Analysis, and Soft Computing. *Foods* **2023**, *12*, 2192. [[CrossRef](#)]
28. Xu, N.; Chen, B.; Sun, H.; Huang, W.; Wu, Y.; Lu, L.; Lou, X.; Xie, C. High-Throughput Phenotyping of Multiple Quantitative Traits for Saffron Corm Rot via NIR Hyperspectral Imaging and Broad Learning System. *Microchem. J.* **2026**, *220*, 116603. [[CrossRef](#)]
29. Verrelst, J.; Malenovský, Z.; Van der Tol, C.; Camps-Valls, G.; Gastellu-Etchegorry, J.P.; Lewis, P.; North, P.; Moreno, J. Quantifying Vegetation Biophysical Variables from Imaging Spectroscopy Data: A Review on Retrieval Methods. *Surv. Geophys.* **2019**, *40*, 589–629. [[CrossRef](#)]
30. Basak, D.; Pal, S.; Patranabis, D.C. Support Vector Regressio. *Neural Inf. Process.-Lett. Rev.* **2007**, *11*, 203–224.
31. Smola, A.J.; Schölkopf, B. A Tutorial on Support Vector Regression. *Stat. Comput.* **2004**, *14*, 199–222. [[CrossRef](#)]
32. Geladi, P.; Kowalski, B.R. Partial Least-Squares Regression: A Tutorial. *Anal. Chim. Acta* **1986**, *185*, 1–17. [[CrossRef](#)]
33. Abdel-Rahman, E.M.; Mutanga, O.; Odindi, J.; Adam, E.; Odindo, A.; Ismail, R. Estimating Swiss Chard Foliar Macro- and Micronutrient Concentrations under Different Irrigation Water Sources Using Ground-Based Hyperspectral Data and Four Partial Least Squares (PLS)-Based (PLS1, PLS2, SPLS1 and SPLS2) Regression Algorithms. *Comput. Electron. Agric.* **2017**, *132*, 21–33. [[CrossRef](#)]

34. dos Santos Neto, J.P.; de Assis, M.W.D.; Casagrande, I.P.; Cunha Júnior, L.C.; de Almeida Teixeira, G.H. Determination of 'Palmer' Mango Maturity Indices Using Portable near Infrared (VIS-NIR) Spectrometer. *Postharvest Biol. Technol.* **2017**, *130*, 75–80. [[CrossRef](#)]
35. Breiman, L. Random Forests. *Mach. Learn.* **2001**, *45*, 5–32. [[CrossRef](#)]
36. Rodriguez-Galiano, V.F.; Ghimire, B.; Rogan, J.; Chica-Olmo, M.; Rigol-Sanchez, J.P. An Assessment of the Effectiveness of a Random Forest Classifier for Land-Cover Classification. *ISPRS J. Photogramm. Remote Sens.* **2012**, *67*, 93–104. [[CrossRef](#)]
37. Pallotti, C.; Renau-Morata, B.; Cardone, L.; Nebauer, S.G.; Albiñana Palacios, M.; Rivas-Sendra, A.; Seguí-Simarro, J.M.; Molina, R.V. Understanding the Saffron Corm Development—Insights into Histological and Metabolic Aspects. *Plants* **2024**, *13*, 1125. [[CrossRef](#)] [[PubMed](#)]
38. Gusain, S.; Joshi, R. Morphological, Physiological, and Transcriptional Changes in *Crocus sativus* L. Under In Vitro Polyethylene Glycol-Induced Water Stress. *Biology* **2025**, *14*, 78. [[CrossRef](#)]
39. Bertoft, E. Understanding Starch Structure: Recent Progress. *Agronomy* **2017**, *7*, 56. [[CrossRef](#)]
40. Pérez, S.; Baldwin, P.M.; Gallant, D.J. Structural Features of Starch Granules I. In *Starch*; Elsevier Inc.: Amsterdam, The Netherlands, 2009; pp. 149–192.
41. Roger, P.; Bello-Perez, L.A.; Colonna, P. Contribution of Amylose and Amylopectin to the Light Scattering Behaviour of Starches in Aqueous Solution. *Polymer* **1999**, *40*, 6897–6909. [[CrossRef](#)]
42. Zeng, L.; Chen, C. Simultaneous Estimation of Amylose, Resistant, and Digestible Starch in Pea Flour by Visible and near-Infrared Reflectance Spectroscopy. *Int. J. Food Prop.* **2018**, *21*, 1129–1137. [[CrossRef](#)]
43. Sims, D.A.; Gamon, J.A. Estimation of Vegetation Water Content and Photosynthetic Tissue Area from Spectral Reflectance: A Comparison of Indices Based on Liquid Water and Chlorophyll Absorption Features. *Remote Sens. Environ.* **2003**, *84*, 526–537. [[CrossRef](#)]
44. Hennessy, A.; Clarke, K.; Lewis, M. Hyperspectral Classification of Plants: A Review of Waveband Selection Generalisability. *Remote Sens.* **2020**, *12*, 113. [[CrossRef](#)]
45. Li, C.; Czyż, E.A.; Halitschke, R.; Baldwin, I.T.; Schaepman, M.E.; Schuman, M.C. Evaluating Potential of Leaf Reflectance Spectra to Monitor Plant Genetic Variation. *Plant Methods* **2023**, *19*, 108. [[CrossRef](#)]
46. Farhadi, R.; Afkari-Sayyah, A.H.; Jamshidi, B.; Mousapour Gorji, A. Prediction of internal compositions change in potato during storage using visible/near-infrared (Vis/NIR) spectroscopy. *Int. J. Food Eng.* **2020**, *16*, 20190110. [[CrossRef](#)]
47. Daughtry, C.S.T.; Hunt, E.R.; McMurtrey, J.E. Assessing Crop Residue Cover Using Shortwave Infrared Reflectance. *Remote Sens. Environ.* **2004**, *90*, 126–134. [[CrossRef](#)]
48. Lamb, B.T.; Dennison, P.E.; Hively, W.D.; Kokaly, R.F.; Serbin, G.; Wu, Z.; Dabney, P.W.; Masek, J.G.; Campbell, M.; Daughtry, C.S.T. Optimizing Landsat Next Shortwave Infrared Bands for Crop Residue Characterization. *Remote Sens.* **2022**, *14*, 6128. [[CrossRef](#)]
49. Sadeghi, A.; Khani, S.; Sabourian, R.; Hajimahmoodi, M.; Ghasemi, J.B. Integrating CNNs and chemometrics for ana-lyzing NIR spectra and RGB images in turmeric adulterant detection. *J. Food Compos. Anal.* **2025**, *141*, 107324. [[CrossRef](#)]
50. Cozzolino, D. The Role of Near-Infrared Sensors to Measure Water Relationships in Crops and Plants. *Appl. Spectrosc. Rev.* **2017**, *52*, 837–849. [[CrossRef](#)]
51. Sun, Y.; Liu, Y.; Yu, H.; Xie, A.; Li, X.; Yin, Y.; Duan, X. Non-Destructive Prediction of Moisture Content and Freezable Water Content of Purple-Fleshed Sweet Potato Slices during Drying Process Using Hyperspectral Imaging Technique. *Food Anal. Methods* **2017**, *10*, 1535–1546. [[CrossRef](#)]
52. Ringsted, T.; Siesler, H.W.; Engelsen, S.B. Monitoring the Staling of Wheat Bread Using 2D MIR-NIR Correlation Spectroscopy. *J. Cereal Sci.* **2017**, *75*, 92–99. [[CrossRef](#)]
53. Cozzolino, D.; Degner, S.; Eglinton, J. A Review on the Role of Vibrational Spectroscopy as an Analytical Method to Measure Starch Biochemical and Biophysical Properties in Cereals and Starchy Foods. *Foods* **2014**, *3*, 605–621. [[CrossRef](#)] [[PubMed](#)]
54. Jin, X.; Shi, C.; Yu, C.Y.; Yamada, T.; Sacks, E.J. Determination of Leaf Water Content by Visible and Near-Infrared Spectrometry and Multivariate Calibration in *Miscanthus*. *Front. Plant Sci.* **2017**, *8*, 721. [[CrossRef](#)]
55. Arefi, A.; Sturm, B.; Hoffmann, T. Explainability of Deep Convolutional Neural Networks When It Comes to NIR Spectral Data: A Case Study of Starch Content Estimation in Potato Tubers. *Food Control* **2025**, *169*, 110979. [[CrossRef](#)]
56. Frey, L.A.; Baumann, P.; Aasen, H.; Studer, B.; Kölliker, R. A Non-Destructive Method to Quantify Leaf Starch Content in Red Clover. *Front. Plant Sci.* **2020**, *11*, 569948. [[CrossRef](#)] [[PubMed](#)]
57. Alsayied, N.F.; Fernández, J.A.; Schwarzacher, T.; Heslop-Harrison, J.S. Diversity and relationships of *Crocus sativus* and its relatives. *Ann. Bot.* **2015**, *116*, 359–368. [[CrossRef](#)] [[PubMed](#)]

**Disclaimer/Publisher's Note:** The statements, opinions and data contained in all publications are solely those of the individual author(s) and contributor(s) and not of MDPI and/or the editor(s). MDPI and/or the editor(s) disclaim responsibility for any injury to people or property resulting from any ideas, methods, instructions or products referred to in the content.